Microscopic identification of stepped SiC(0001) and the reaction site of hydrogen-rich epitaxial growth

Tomoya Kimura,[1,*] Kenta Chokawa,[2,†] Kenji Shiraishi,[1,2] and Atsushi Oshiyama[2]
[1]*Graduate School of Engineering, Nagoya University, Furo-cho, Chikusa-ku, Nagoya 464-8603, Japan*
[2]*Institute of Materials and Systems for Sustainability, Nagoya University, Furo-cho, Chikusa-ku, Nagoya 464-8601, Japan*

(Received 8 February 2022; accepted 11 July 2022; published 26 July 2022)

We report first-principles total-energy electronic-structure calculations, based on density-functional theory, that unveil detailed atomic structures of hydrogen-adsorbed step edges and their energetics of the silicon carbide (SiC) (0001) surface. The obtained adsorption energy of the hydrogen atom at each step reveals the microscopic reason for the step morphology on the Si-face SiC(0001) surfaces which are commonly inclined toward the $\langle 11\bar{2}0\rangle$ direction in epitaxial growth. The calculated hydrogen coverages at each step and also on the surface terrace clearly identify the favorable reaction sites for the epitaxial growth, such as chemical vapor deposition (CVD) in which hydrogen is ubiquitous. The obtained results provide a firm theoretical framework to discuss the atom-scale mechanism of the epitaxial growth of SiC.

DOI: 10.1103/PhysRevB.106.035309

I. INTRODUCTION

Silicon carbide (SiC) is a material that has been studied for more than a century [1,2] and has been widely used as hard ceramics. It is now emerging as a material for power electronics in semiconductor technology due to its superior properties such as wide band gap, high electric breakdown voltage, and robustness under a harsh environment, compared with the current principal material, Si [3]. Actually, SiC power devices such as metal-oxide-semiconductor field-effect transistors (MOSFETs) are already on the market and have been introduced in railways and electric vehicles [4]. However, the performance of the current SiC devices are still lower than what is expected from its intrinsic superior properties. The reason is presumably the lack of optimization of the fabrication processes of the devices.

Among various fabrication processes, epitaxial growth of thin films of target semiconductors [3–5] is primary to assure the high quality of electron devices. In the epitaxial growth of semiconductors, foreign species arrive at growth surfaces usually from the gas phase and are incorporated in crystalline thin films. Atomic reactions through this growth processes were rarely addressed in the past but their clarification is strongly demanded in the current nanometer-scale technology. Furthermore, the microscopic identification of the stage, i.e., the stepped surface, for the epitaxial growth is an inevitable prerequisite to be clarified.

The current technique for epitaxial growth of SiC is chemical vapor deposition (CVD) at around 1600 °C [6], in which silane (SiH_4) and propane (C_3H_8) are used as gas sources for the synthesis of SiC with hydrogen (H_2) molecules carrying those gas sources. Such CVD has been improved by the addition of hydrogen chloride (HCl). This addition of HCl to CVD, called halide CVD (HCVD), certainly increases the growth rate and improves the quality of thin films [7]. Reactions of those molecules in the gas phase have been recently studied by density-functional calculations combined with an independent molecule model under typical growth conditions such as growth temperature at around 1625 °C [8] and respective vapor pressure of each gaseous molecule [9]. It is then revealed that $SiCl_2$ and C_2H_2 molecules along with H_2 are a majority in the gas phase. Hence the HCVD growth of SiC is expected to occur with $SiCl_2$ and C_2H_2 on hydrogen-covered SiC surfaces. [The H coverage on SiC(0001) depends on temperature and the partial pressure and will be discussed in detail in Sec. III C.]

The epitaxial growth usually takes place on the vicinal surface in which the surface normal is inclined by a few degrees toward a particular direction perpendicular to the normal: e.g., in SiC(0001) CVD, the growth surface is typically inclined toward the $\langle 11\bar{2}0\rangle$ direction [3]. The resulting growth surface thus consists of flat terraces and atom-scale steps and the epitaxial growth takes place through the incorporation of foreign species mainly at the step edges (step-flow growth [6,10]). Hence the identification of the step-edge structures is the first priority to reveal the microscopic mechanism of the epitaxial growth. In addition to that, the morphology of the step edges in the nanometer scale, such as straight or meandering shape, is interesting in condensed-matter science and also important in the epitaxial growth. Such morphology should be determined by the energetics and kinetics of the step edges. For the hydrogen-free SiC(0001) surfaces, the energetics of the step-edge structures and the resulting morphology have been recently clarified by density-functional calculations [11,12]. Clarification of the energetics of the *hydrogen-covered* SiC(0001) stepped surfaces which are more realistic under actual growth conditions [8,9] has not been achieved yet and is certainly inevitable.

From another viewpoint, SiC is an ambivalent material in which covalency is a main characteristic in determining

[*]Present address: DENSO Corporation, Kariya, Japan.
[†]Present address: KIOXIA Corporation, Yokkaichi, Japan.

 ©2022 American Physical Society

physical properties but also ionicity, i.e., the electron transfer from Si to C, plays an important role, bridging typical elemental semiconductors such as Si and Ge and III-V compound semiconductors. This ambivalence manifests itself in the surface step structures and the energetics of the H adsorption, which we discuss below.

In this paper, we perform first-principles calculations based on density-functional theory (DFT) [13,14], microscopically identify step-edge structures, and reveal the energetics of the hydrogen-rich SiC(0001). The obtained results for the hydrogen adsorption energies, and thus the hydrogen coverage for particular adsorption sites at the step edges as well as on the surface terrace, unequivocally identify the stage of the SiC epitaxial growth.

The organization of the present paper is as follows. In Sec. II A, details of step edges on SiC(0001) vicinal surfaces are described. In Secs. II B–II D, our density-functional calculations combined with thermodynamic analysis are explained. Calculated results for the energetics of H-adsorbed step-edge structures and the resulting step morphology are presented in Secs. III A and III B. Discussion on the growth processes based on the calculated hydrogen coverages of each step is given in Sec. III C. Our findings are summarized in Sec. IV.

II. COMPUTATIONAL METHODS

A. Classification of step edges on the (0001) vicinal surfaces

We start with the classification of step edges on SiC(0001) surface inclined toward either the $\langle 11\bar{2}0\rangle$ or $\langle 1\bar{1}00\rangle$ direction. The atomic height of the step edge is not clearly identified in microscopy or spectroscopy measurements. However, recent first-principles calculations have shown that the monobilayer atomic step is energetically favorable [15,16]. This is due to the fact that structural relaxation near step edges in the clifflike higher steps is infeasible. We thus focus on the monobilayer steps in this paper.

Figure 1 shows a schematic view of the hydrogen-free monobilayer steps. Along the $\langle 1\bar{1}00\rangle$ direction, four distinct edges of monobilayer steps appear: They are labeled as Si2(C2) and Si3(C1) in which Si (C) atoms appear at the edges with one, two, or three dangling bonds before structural relaxation (Fig. 1). Along the $\langle 11\bar{2}0\rangle$ direction the edge shape is unique, labeled as SC in which both Si and C atoms appear at the edge. It is of note that Si2 becomes C2 upon removal of the edge Si and vice versa, and that Si3 and C1 have a similar relation (Fig. 1). Recent density-functional calculations for the H-free surface [11,12] have found structural relaxation patterns peculiar to each step edge: the rebonding between the lower- and the upper-terrace Si atoms for the Si2 and the SC, and the resonant bonding [17,18] for the Si3. This peculiar relaxation determines the order of the step formation energies, leading to an argument that the step toward $\langle 11\bar{2}0\rangle$ is not straight consisting only of the SC edges, but is meandering with the Si2 and the Si3 edges. The meandering of the step edges is occasionally observed in experiments [19–22].

In experiments, especially epitaxial growth experiments such as HCVD, however, hydrogen is ubiquitous and the growth surface is expected to be covered by hydrogen. There is thus a great need to identify step structures with hydrogen

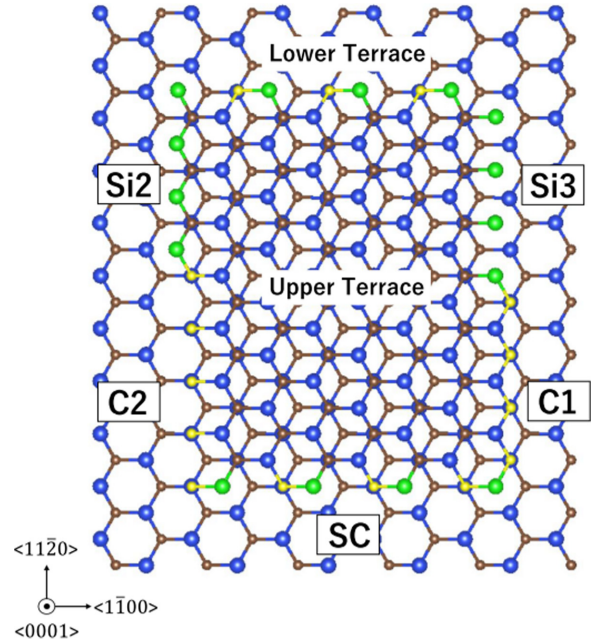

FIG. 1. Schematic view of the five distinct monobilayer steps on SiC(0001) surface. Blue and brown balls depict Si and C atoms, respectively. The edge Si and C atoms are represented by green and yellow balls, respectively. The SC step along the $\langle 1\bar{1}00\rangle$ direction and the Si2, Si3, C1, and C2 steps along the $\langle 11\bar{2}0\rangle$ direction are shown all together.

and determine their energetics. Although the growth typically takes place on the vicinal surface inclined toward the $\langle 11\bar{2}0\rangle$ direction [3], examining all five step edges is important in discussing the step morphology and atomic reactions on the terrace, the step edge, and the kinks.

B. Density-functional calculations

All calculations are performed based on DFT with the Kohn-Sham scheme using the Vienna *ab initio* simulation package (VASP) [23–26]. In this calculation, we use the Perdew-Burke-Ernzerhof (PBE) generalized gradient approximation [27] for the exchange-correlation energy functional. Interactions between the ionic cores and the valence electrons are described by the projected augmented-wave potential [28]. The cutoff energy for the plane-wave basis is 500 eV. The Brillouin-zone (BZ) integration is performed with Monkhorst-Pack k-point sampling [29]. In calculations for bulk 4H-SiC with a primitive cell, we use $6 \times 6 \times 2$ sampling points in BZ integration. With those calculational parameters, the obtained lattice constants a, b, and c and the bulk modulus B_0 of 4H-SiC are $a = b = 3.094$ Å, $c = 10.13$ Å, and $B_0 = 211$ Pa. These values are in good agreement with the experimental values within 0.8%, 0.2%, and 3.2%, respectively [30]. The geometry optimization is performed until all the atomic forces become less than 0.05 eV Å^{-1}.

C. Slab models

To simulate stepped and flat surfaces, we use a repeating slab model in which each slab is separated from its image

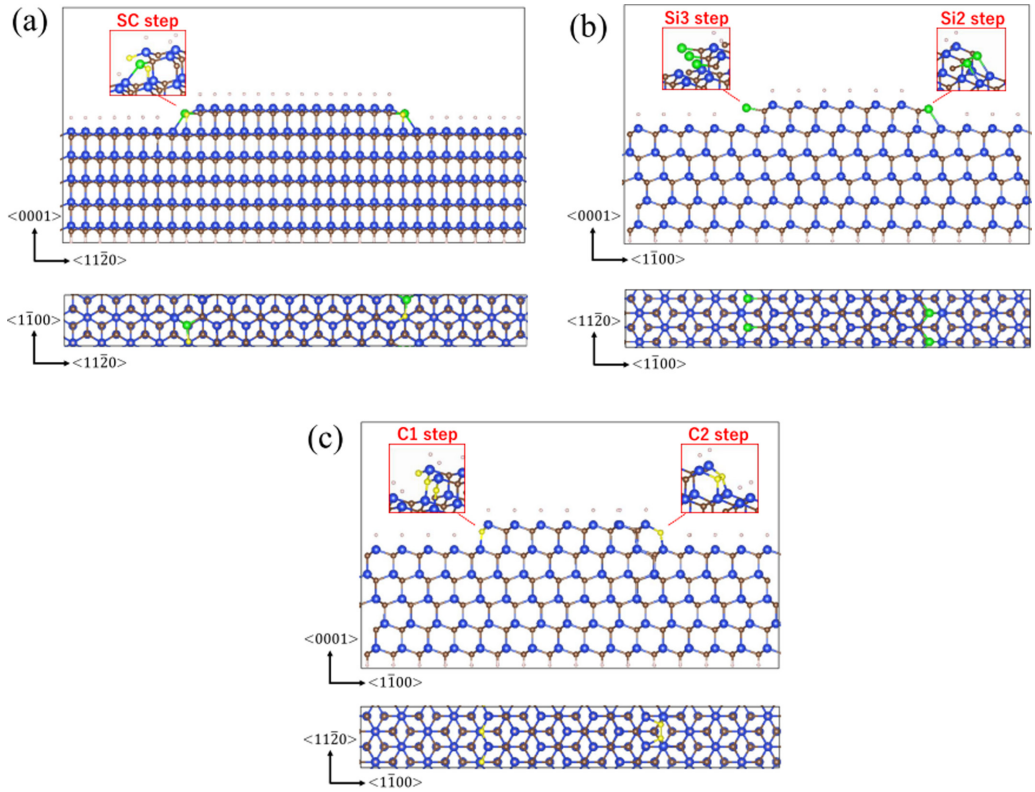

FIG. 2. Side and top views of the periodic-array slab models in which an upper terrace and a lower terrace appear alternately. (a) SC steps, (b) a Si2 step and a Si3 step, and (c) a C1 step and a C2 step on the 4H-SiC(0001) surfaces. The color code is the same as in Fig. 1. Pink balls are H atoms.

slabs by the vacuum layers with thickness of more than 10 Å. The bottom of the slab is terminated by H atoms which are fixed and thus mimic the substrate. The step is described by a periodic-array slab (Fig. 2) in which an upper and a lower terrace with two step edges appear alternately in a lateral direction. The upper- and the lower-terrace parts are composed of six and five bilayers, respectively. In the geometry optimization, the bottom two SiC bilayers are fixed to their bulk positions. As for the step toward $\langle 11\bar{2}0\rangle$, the two step edges are both SC [Fig. 2(a)]. For the step toward $\langle 1\bar{1}00\rangle$, we choose two pairs, i.e., Si2 + Si3 [Fig. 2(b)] and C1 + C2 [Fig. 2(c)] to explore the characteristics of Si-edge and C-edge atoms. The lateral cells in the slab models with the $\langle 11\bar{2}0\rangle$ and $\langle 1\bar{1}00\rangle$ steps have the periodicity of $(\sqrt{3}\times 16)$ and $(2\times 8\sqrt{3})$, respectively, following previous reports in the literature [11,12]. Consequently, our periodic-array slabs for the SC-SC pair and the Si2-Si3 and C1-C2 pairs have the dimensions of (5.4×49.5) Å^2 and (6.2×42.9) Å^2, respectively, in the lateral plane and 25.3 Å along the c direction. BZ integration is performed with the $2\times 1\times 1$ Monkhorst-Pack k points.

When we examine the hydrogen adsorption at the step edge, we choose a single step edge in the periodic-array slab (Fig. 2) and consider all the possible geometries with H atoms adsorbed, leaving the other step edge hydrogen free and fixed. The dangling bonds on the (0001) surface terraces, except near the edges, are also terminated by hydrogen atoms. We perform geometry optimization and obtain the H-adsorption energy for all the possible step edges.

In addition, to discuss the hydrogen adsorption on the 4H-SiC(0001) surface terrace in Sec. III C, we have prepared a slab model for the flat surface with the (1×1) lateral periodicity. For Brillouin-zone integration, we use the $16\times 16\times 2$ Monkhorst-Pack k points. The atomic configurations used in this paper are drawn using VESTA [31].

D. Hydrogen adsorption energy

We compare the stabilities of H-adsorbed structures of each step by calculating the hydrogen adsorption energy $\Delta E^0_{\rm ad}$:

$$\Delta E^0_{\rm ad} = -\left[E_{\rm H_{ad}} - \left(E_0 + n_{\rm H}\mu^0_{\rm H}\right)\right], \tag{1}$$

where E_0 is the total energy of the slab model before hydrogen adsorption on the step, $E_{\rm H_{ad}}$ is the total energy after $n_{\rm H}$ hydrogen atoms are adsorbed on the step, and $\mu^0_{\rm H}$ is the chemical potential of the H atom. In this paper we regard $\mu^0_{\rm H}$ as being half of the H_2 molecular energy.

To discuss the hydrogen coverage on the 4H-SiC(0001) surface at growth conditions in Sec. III C, we also calculate the hydrogen adsorption energy $\Delta E_{\rm ad}(T,P)$ by introducing the Gibbs free energy per atom of an H_2 molecule $\mu_{\rm H}(T,P)$ at finite temperature T and the partial pressure P by using the following equations obtained from an independent molecule model:

$$\Delta E_{\rm ad}(T,P) = -\{E_{\rm H_{ad}} - [E_0 + n_{\rm H}\mu_{\rm H}(T,P)]\}, \tag{2}$$

$$\mu_{\rm H}(T,P) = \frac{1}{2}\left[\mu^0_{\rm H_2} - k_{\rm B}T\,\ln\left(\frac{k_{\rm B}T}{P}\times\zeta_{\rm trans}\zeta_{\rm rot}\zeta_{\rm vibr}\right)\right], \tag{3}$$

$$\zeta_{\rm trans} = \left(\frac{2\pi m k_{\rm B} T}{h^2}\right)^{\frac{3}{2}}, \tag{4}$$

$$\zeta_{\rm rot} = \frac{1}{\pi\sigma}\frac{8\pi^3 I k_{\rm B} T}{h^2}, \tag{5}$$

$$\zeta_{\rm vibr} = \frac{1}{1-\exp\left(-\frac{h\nu}{k_{\rm B}T}\right)}, \tag{6}$$

where $\zeta_{\rm trans}$, $\zeta_{\rm rot}$, and $\zeta_{\rm vibr}$ are the partition functions for the translational, the rotational, and the vibrational motions, respectively. Here, $k_{\rm B}$ is Boltzmann's constant, m is the mass of H_2, h is Planck's constant, σ is the symmetric factor of an H_2 molecule, I is the moment of inertia of an H_2 molecule, and ν is the frequency of the vibrational mode of H_2 [32–35].

III. RESULTS AND DISCUSSIONS

A. Hydrogen-adsorbed step-edge structures

Since the epitaxial growth takes place usually on the $\langle 11\bar{2}0\rangle$ vicinal surface, we completely explore hydrogen adsorption sites and the number of adsorbed H atoms at the SC step edge. Taking the double periodicity along the step-edge direction (see Fig. 1), there are five distinct sites for the single-H adsorption: two sites on the upper-terrace Si [Figs. 10(a) and 10(b) in the Appendix], one site that forms a Si-H-Si bridge between the upper- and lower-terrace Si atoms [Fig. 10(c)], one site on the lower-terrace Si [Fig. 10(d)], and one site on the edge C [Fig. 10(e)]. Hence the number of adsorbed H atoms at the SC edge could be up to five and the number of the configurations with many H atoms is huge. However, by consideration of the space accommodating H atoms, many of those H configurations are hindered, and we have found 19 possible structural candidates (not shown): eight configurations for two H atoms, five configurations for three H atoms, and one configuration for four H atoms, in addition to the five configurations (Fig. 10) for a single H atom. We have performed the geometry optimization for the above 19 candidates and found nine stable structures: three for the single-H adsorption (labeled as SC[H1-A], SC[H1-B], and SC[H1-C] hereafter), three for the two-H adsorption (SC[H2-A], SC[H2-B] and SC[H2-C]), twofor the three-H adsorption (SC[H3-A] and SC[H3-B]), and one for the four-H adsorption (SC[H4]) (shown in Fig. 3 and Fig. 11). Each candidate is converted upon the optimization to one of those nine structures. The calculated adsorption energies $\Delta E^0_{\rm ad}$ and the energy per adsorbed H atom $\Delta E^0_{\rm ad}/n_{\rm H}$ for the nine stable structures are shown in Table I.

The calculated $\Delta E^0_{\rm ad}$ shows the maximum value of 3.28 eV for the four-H adsorption, SC[H4], indicating that the adsorption with more H atoms at the step edges is generally favorable. Yet the adsorption energy per H atom, $\Delta E^0_{\rm ad}/n_{\rm H}$, provides more important information. The nine stable adsorbed structures are classified into two groups: One group shows the adsorption energy per H atom being about 1 eV or more, while the other group shows it being about a half eV or less. The former includes SC[H1-A], SC[H2-A], SC[H2-B], and SC[H4]. The optimized geometries for the former group are shown in Fig. 3 and the latter group are shown in Fig. 11 in the Appendix. The reason for the larger H-adsorption energy

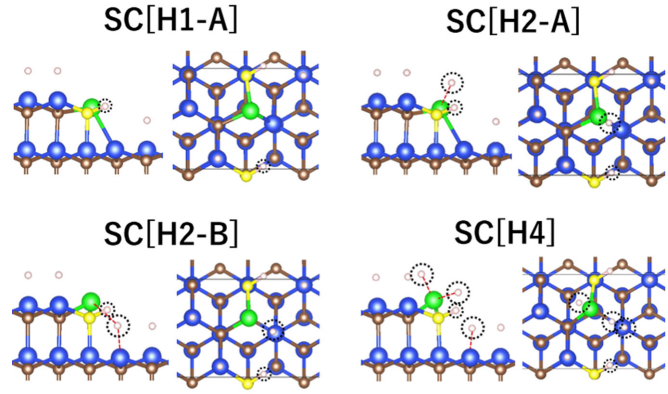

FIG. 3. Side (left) and top (right) views of the optimized local atomic structures of the stable H-adsorbed SC steps with the adsorption energies $\Delta E^0_{\rm ad}/n_{\rm H}$ about 1 eV or more (Table I). Blue, brown, green, yellow, and pink spheres represent Si atoms, C atoms, Si edge atoms, C edge atoms, and H atoms, respectively. H atoms adsorbed on the step edge are circled by the black dotted line.

in the former group is the presence of the C-H bonds at the step edge, as is clearly shown in Fig. 3. In the latter group, the C-H bond is absent (Fig. 11). This difference in the adsorption energy comes from the fact that the bonding energy of C-H is much larger than that of Si-H. The cohesive energies calculated in the present DFT scheme are indeed 18.4 and 13.6 eV for methane, CH_4, and silane, SiH_4, respectively. Hydrogen is adsorbed preferably at the edge C atoms of the SC step.

At this point, we note that the adsorption energy for SC[H1-A] where a single H is adsorbed at the C site is 1.20 eV, significantly smaller than a quarter of the cohesive energy of CH_4. The reason is, we argue, the ionicity in the host SiC. For the H-free SC step, both Si and C dangling bonds (three-fold coordinated edge atoms) appear. Due to the partially ionic character of SiC, the electron is transferred from the Si dangling bond to the C dangling bond, thus stabilizing the structure. This situation is similar to the electron counting rule [36,37] which is one of the main sources to stabilize surface or defect structures in partially ionic compound semiconductors. SiC is a bridging semiconductor between purely covalent group IV elemental semiconductors and substantially ionic compound semiconductors. Upon H adsorption at the edge C atom, this electron transfer is suppressed and the resulting energy loss partly compensates the energy gain upon the H adsorption, though it is not evidenced by explicit computations in the present work.

The structure in which H bridges the upper- and the lower-Si atoms is least energetically favorable though it is certainly found to be metastable (SC[H1-C] in Fig. 11). This higher energy is presumably due to the lack of capability of an H atom to form the multiple bonding. This bridging-type structure, however, is speculated to play a role as a transition state in reactions near the SC step edge, as demonstrated theoretically in the epitaxial growth of GaN [38].

The steps toward the $\langle 1\bar{1}00\rangle$ direction are also important even on the $\langle 11\bar{2}0\rangle$-inclined surface since the steps may be meandering or the step kinks may appear. For the Si-edged steps, Si2 and Si3, there are four possible sites for the single H atom adsorption, i.e., two sites on the upper-terrace edge Si,

TABLE I. Calculated hydrogen adsorption energy ΔE^0_{ad} at monobilayer step edges on the SiC(0001) surface. All the stable H-adsorbed steps found in the present calculation are shown with the number of adsorbed H atoms n_H. The adsorption energy per H atom $\Delta E^0_{ad}/n_H$ is also shown.

	Number of H adsorbed	Adsorption energy (eV)	
Step edge	n_H	ΔE^0_{ad}	$\Delta E^0_{ad}/n_H$
SC H1-A	1	1.20	1.20
H1-B	1	0.52	0.52
H1-C	1	−0.09	−0.09
H2-A	2	2.80	1.40
H2-B	2	1.87	0.94
H2-C	2	1.23	0.62
H3-A	3	1.76	0.59
H3-B	3	0.89	0.30
H4	4	3.28	0.82
Si2 H1-A	1	1.40	1.40
H1-B	1	0.29	0.29
H2-A	2	3.01	1.51
H2-B	2	1.90	0.95
H2-C	2	1.32	0.66
H2-D	2	0.82	0.41
H3-A	3	1.88	0.63
H3-B	3	0.99	0.33
H4	4	1.37	0.34
Si3 H1-A	1	0.40	0.40
H1-B	1	0.05	0.05
H2-A	2	1.32	0.66
H2-B	2	1.01	0.51
H2-C	2	0.02	0.01
H3-A	3	0.86	0.29
H3-B	3	0.14	0.05
H4	4	0.27	0.07
C1 H1	1	2.30	2.30
H2	2	4.65	2.33
C2 H1	1	0.51	0.51
H2	2	2.91	1.46

a single site on the lower-terrace edge Si, and the bridging site between the upper- and the lower-terrace Si atoms (similar to the case of the SC step as in Fig. 10). Our geometry optimization reveals that only two of the four candidates are stable: i.e., the site on the upper-terrace edge Si and the site on the lower-terrace edge Si, labeled as Si2[H1-A], Si2[H1-B], Si3[H1-A], and Si3[H1-B] (Fig. 4). The adsorption energies are found to be substantially different for the upper-terrace and the lower-terrace Si. The calculated $\Delta E^0_{ad}/n_H$ for the upper-terrace edge Si is 5 times (8 times) larger than that for the lower-terrace edge Si for the Si2 (Si3) step (Table I). This is due to the geometrical flexibility for the adsorbed H on the upper-terrace edge Si, as is demonstrated in Fig. 4. In particular, the small adsorption energy in Si3[H1-B] comes from the cleavage of the rebond between the upper- and the lower-edge Si atoms.

The many-H adsorption for the Si2 and the Si3 steps is the combination of the adsorbed structures on the upper and the lower Si edge atoms. From the two-H adsorption to

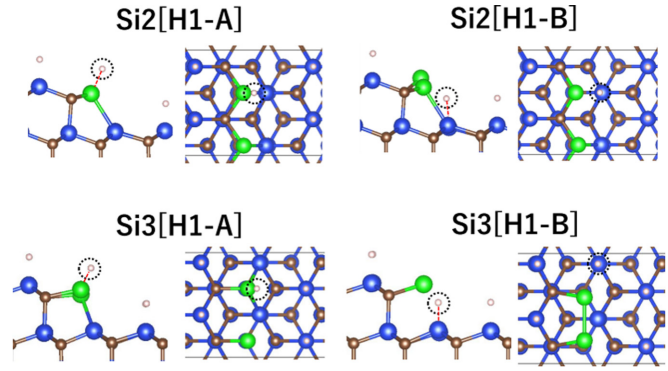

FIG. 4. Side (left) and top (right) views of the local atomic structures of the stable Si2 (upper figures) and Si3 (lower figures) steps with single H atom adsorption. The color code is same as in Fig. 3. H atoms adsorbed on the step edge are circled by the black dotted line.

the four-H adsorption, we have fully examined seven (six) candidate structures for the Si2 (Si3) step edges, performed the geometry optimization for all the structures, and calculated the adsorption energies. All the results are shown in Figs. 12 and 13 in the Appendix for the structures and in Table I for the adsorption energies, along with the results for the single H adsorption. The stable structures for the many-H adsorption are labeled as Si2[H2-A], Si2[H2-B], Si2[H2-C], Si2[H2-D], Si2[H3-A], Si2[H3-B], and Si2[H4] for the Si2, and Si3[H2-A], Si3[H2-B], Si3[H2-C], Si3[H3-A], Si3[H3-B], and Si3[H4] for the Si3, which manifest the step specification, the number of H atoms, and the distinction in structure. As stated above, the H adsorption on the upper-terrace Si edge atom is energetically favorable. The structures Si2[H1-A], Si2[H2-A], Si3[H1-A], and Si3[H2-A] belong to such case, showing larger adsorption energies indeed obtained in the present calculation [Table I, and Figs. 5(a) and 12].

The mixture of the adsorption sites on the upper and the lower terrace forms the next stable structures. Several different configurations show distinct structures and respective adsorption energies. The differences in the obtained adsorption energies, e.g., Si2[H2-B] and Si2[H2-D] [Figs. 5(b) and 5(c)], are ascribed to another physical reason: i.e., the preserving or the cleavage of the rebonds between the upper- and lower-terrace Si atoms which are a major source of the stabilization of the H-free step edges [10,11]. The cleavage is certainly a source of the energy increase and we observe such case in our obtained structures, Si2[H2-B] vs Si2[H2-D], Si2[H3-A] vs Si2[H3-B], and Si3[H2-B] vs Si3[H2-C] (Figs. 12 and 13, and Table I).

For the Si3 step, the situation is similar to the Si2 step. Yet, we have found that the H adsorption energies at the Si3 step edge are small compared with those at the SC and the Si2. These small adsorption energies are due to the interference in the formation of the Si-H bonds and the resonantlike bonds inherent to Si3. The small adsorption energy leads to the small H coverage, thus rendering Si3 important in growth reaction (see below).

Structural relaxation near the C1 step is almost absent in the H-free case [11,12], leaving the edge C threefold coordinated with the dangling bond directed toward the open

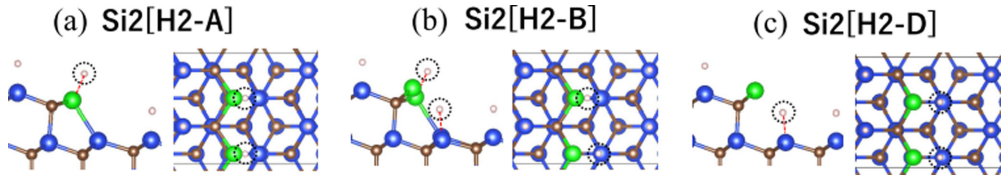

FIG. 5. Side (left) and top (right) views of the local atomic structures of the stable Si2 steps with two H atom adsorption. (a) The most stable structures. (b,c) The stable structures with and without the rebonding between the upper and the lower Si atoms. The color code for the atoms is the same as in Fig. 3. H atoms adsorbed on the step edge are circled by the black dotted line.

space. Hence the only plausible way to get H adsorption is the termination of this dangling bond. We have taken the double periodicity along the step edge (two edge C atoms in a cell) and indeed found stable single-H and two-H adsorbed structures **[**C1[H1] and C1[H2] structures in Figs. 6(a) and 6(b)**]**. The calculated adsorption energies per H atom for the two cases are close to each other and the largest among various adsorbed structures (Table I), reflecting the strong C-H bond. For the C2 step, some interesting structural variants are possible. In the H-free case, two of the twofold coordinated C edge atoms form a carbon dimer, gaining the energy. The C-C bond length at the H-free C2 step is 1.47 Å, which is shorter than that in the crystalline diamond of 1.54 Å. This indicates that the C-C bond at the H-free C2 step is a double bond with σ plus π characteristics. In the H atmosphere, two possibilities emerge: H being adsorbed at the threefold coordinated C atom of the dimer or breaking the C dimer intervening into the edge C-C dimerized bond. We have performed structural optimization for those candidate structures and found the most stable structures, shown in Figs. 6(c) and 6(d): The H atoms are adsorbed at one of the threefold coordinated C atoms of the dimer **[**C2[H1] in Fig. 6(c)**]** or at both of the dimerized atoms **[**C2[H2] in Fig. 6(d)**]**. The latter is energetically more favorable because of the annihilation of the threefold coordinated C atoms. Yet it is noteworthy that the adsorption energy per H atom is substantially smaller than a quarter of the cohesive energy of CH_4 due to the annihilation of the double bond (the C-C distance in C2[H2] is 1.63 Å).

The calculated adsorption energies shown in Table I do not include the contribution from the zero-point energy (ZPE) of the H vibration. The ZPEs, E^{ZPE}, are expected to be sizable for the H vibration: The calculated values in the present scheme for an H_2 molecule, and the CH and SiH bonds at each step are $E^{\mathrm{ZPE}}_{\mathrm{H_2}} = 0.270$ (eV), $E^{\mathrm{ZPE}}_{\mathrm{CH}} = 0.170$ (eV), and $E^{\mathrm{ZPE}}_{\mathrm{SiH}} = 0.122$ (eV), respectively. It is of note that the ZPE calculations of the CH and SiH bonds have been performed by treating them as CH and SiH molecules, respectively. We have then calculated the adsorption energies for the ten most stable sites, SC[H1-A], SC[H2-A], Si2[H1-A], Si2[H2-A], Si3[H2-A], Si3[H2-B], C1[H1], C1[H2], C2[H1], and C2[H2], taking into account the ZPE contributions. The obtained values are essentially the same as the values without ZPE in Table I: The difference in the adsorption energy per H atom is 70 meV at most. This is due to the fact that ZPEs in an H_2 molecule and in the adsorbed structures are similar to each other and each contribution cancels out.

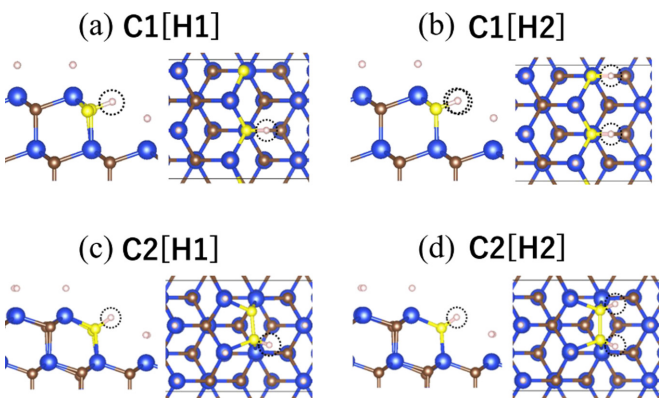

FIG. 6. Side (left) and top (right) views of the local atomic structures of the geometry-optimized H-adsorbed C1 and C2 steps. The color code is the same as in Fig. 3. H atoms adsorbed on the step edge are circled by the black dotted line.

Our density-functional calculations presented above have identified 30 stable H-covered SiC step structures among numerous candidate structures, and provide quantitative adsorption energy for each step structure. This unveils underlying physics and chemistry which determine the energetics of the H-covered surface steps on SiC(0001) characterized as the coexistence of covalency and ionicity. The obtained results are certainly basics in considering the step-flow mode of the epitaxial growth. Experimental evidence for the structures predicted in the present work is awaited.

B. Step morphology during the epitaxial growth

Recent DFT calculations for the $\langle 11\bar{2}0\rangle$-inclined (0001) surfaces have clarified that the morphology of the steps is not straight but meandering under the H-free condition [11,12]: The total-energy calculations have shown that the meandering (zigzag) step consisting of the Si2 and Si3 step edges [Fig. 7(a)] is lower in the formation energy than the straight step consisting of the SC step edge alone [Fig. 7(b)]. The step formation energy for the straight step with respect to that of the zigzag step, $\Delta\lambda_{\mathrm{H_{free}}}$, is calculated to be $0.05 - 0.13$ eV Å^{-1} (corresponding to $0.1 - 0.2$ eV per edge Si atom), depending on the Si chemical potential μ_{Si} or the C chemical potential μ_{C}. The μ_{Si} is in the range of $-\Delta H_f \leqslant \mu_{\mathrm{Si}} \leqslant \varepsilon_{\mathrm{Si\ crystal}}$ under the condition of $\mu_{\mathrm{Si}} + \mu_{\mathrm{C}} = \varepsilon_{\mathrm{SiC}}$ where $\varepsilon_{\mathrm{Si\ crystal}}$ and $\varepsilon_{\mathrm{SiC}}$ are the energies of crystalline Si and SiC, respectively, and ΔH_f is the heat of formation of SiC. The lower and the upper limits of μ_{Si} correspond to Si-poor and -rich conditions, respectively, and the upper limit of $\Delta\lambda_{\mathrm{H_{free}}}$ corresponds to the Si-rich condition.

We are now in a position to discuss the effects of H adsorption on the step morphology. Based on previous reports in the

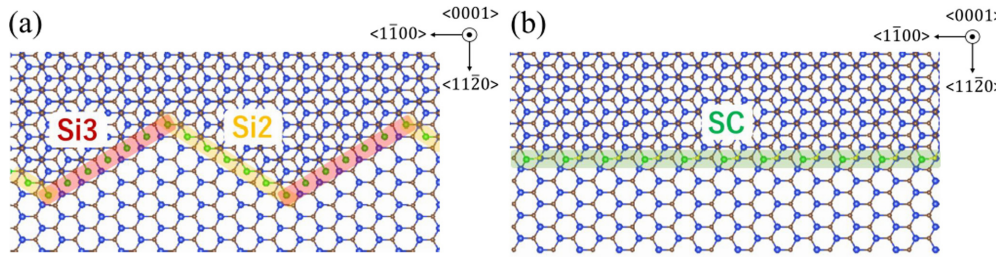

FIG. 7. Top views of the zigzag (a) and straight (b) step edges toward $\langle 11\bar{2}0\rangle$ directions on SiC(0001) surface. The color code of the atom representation is the same as in Fig. 2.

literature [11,12], the formation-energy difference $\Delta\lambda_{H_{ad}}$ for the H-covered step is given by

$$\Delta\lambda_{H_{ad}} = \Delta\lambda_{H_{free}} + E_{corr}, \tag{7}$$

where E_{corr} is the correction term due to the H adsorption on the step edges, and is written as

$$E_{corr} = -\frac{N^{SC}_{unit}\Delta E^{SC}_{ad} - \left(N^{Si2}_{unit}\Delta E^{Si2}_{ad} + N^{Si3}_{unit}\Delta E^{Si3}_{ad}\right)}{l_{SC}}. \tag{8}$$

Here l_{SC} is the length of the straight SC step that constitutes the Si2 + Si3 zigzag step; N^{SC}_{unit}, N^{Si2}_{unit}, and N^{Si3}_{unit} are the number of the SC, Si2, and Si3 step units present in those steps; ΔE^{SC}_{ad}, ΔE^{Si2}_{ad}, and ΔE^{Si3}_{ad} are the H-adsorption energies on the SC, Si2, and Si3 step units obtained by Eq. (1), which have been calculated in the previous subsection. In this section, we focus on the step structures with the large adsorption energy per H atom $\Delta E^{0}_{ad}/n_H$: i.e., SC[H2-A] for the SC step, Si2[H2-A] for the Si2 step, and Si3[H2-A] for the Si3 step. It is of note that the relative stability of the straight vs zigzag-shaped steps represented by Eqs. (7) and (8) is independent of the hydrogen chemical potential μ^0_H since the number of H atoms is the same in the models for straight and zigzag shapes.

The calculated formation-energy differences for those H-covered steps $\Delta\lambda_{H_{ad}}$ are $-0.07 - 0.01$ eV Å^{-1}, depending on the Si chemical potential. In the Si-poor condition, $\Delta\lambda_{H_{ad}}$ is a negative value, which means that the H-adsorbed SC straight step is more energetically favorable than the H-adsorbed Si2 + Si3 zigzag-shaped step. Hence, the SC straight step is likely to appear on the vicinal surface under the Si-poor conditions during H-rich CVD growth. On the other hand, in the Si-rich condition, $\Delta\lambda_{H_{ad}}$ is positive and the formation energy of the H-adsorbed Si2 + Si3 zigzag-shaped step is lower than that of the H-adsorbed straight SC step. Hence, the Si2 + Si3 zigzag-shaped step tends to appear on the surface. From these results, when the energetics rather than the kinetics is important, it is concluded that the morphology of the steps on the SiC(0001) vicinal surface inclined along the $\langle 11\bar{2}0\rangle$ direction can be controlled by varying the growth conditions from Si poor to Si rich.

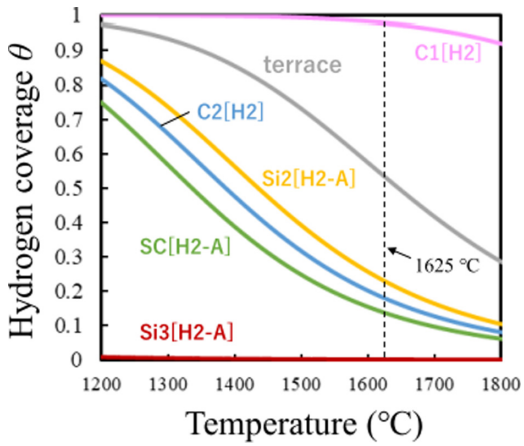

FIG. 8. Hydrogen coverage of terrace and steps as a function of temperature at $P_H = 0.25$ atm.

C. Hydrogen coverage

We next examine the hydrogen coverage at each step edge and on the (0001) surface terrace to discuss the step-flow growth mode under actual growth conditions. The coverage θ is rigorously obtained by the derivative of the grand partition function Ξ with respect to the chemical potential of hydrogen

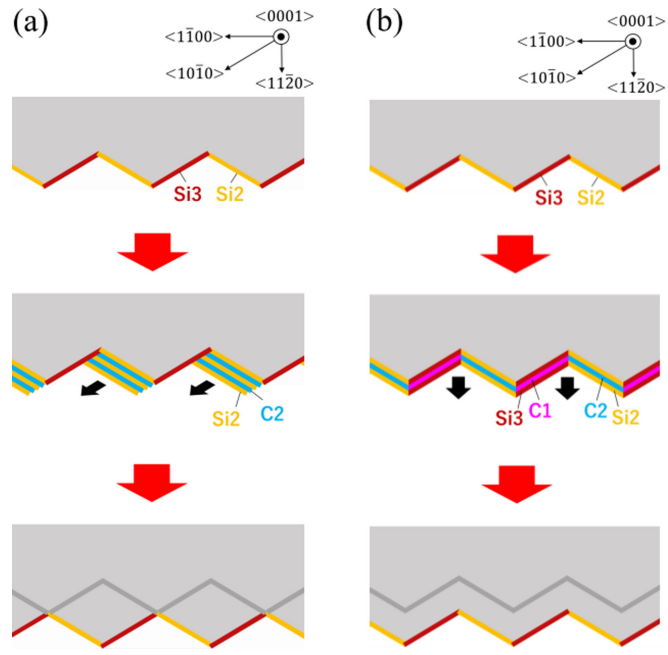

FIG. 9. Schematic illustration of the epitaxial growth of Si2 + Si3 zigzag-shaped step edge. (a) In the case that the growth rate for the Si2/C2 side overwhelms that of the Si3/C1 side. (b) In the case that the growth rates at the Si2/C2 side and the Si3/C1 side are comparable. The variation of the position of the growth-front kinks is different in the step-size scale in (a,b).

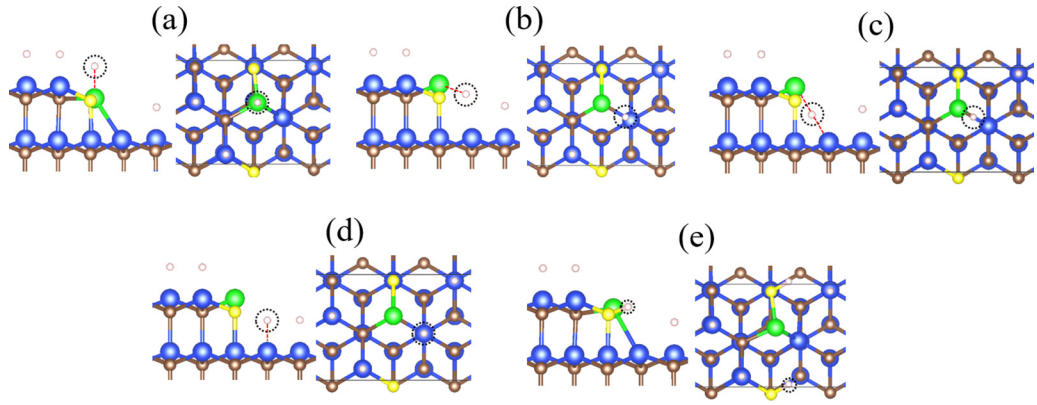

FIG. 10. Side (left) and top (right) views of the five distinct configurations for the single H adsorption at the SC step edge before structural relaxation. (a) On the upper-edge Si, (b) at the upper-edge Si, (c) bridging, (d) on the lower-edge Si, and (e) at the edge C. Blue, brown, green, yellow, and pink balls represent Si atoms, C atoms, Si edge atoms, C edge atoms, and H atoms, respectively. H atoms adsorbed on the step edge are circled by the black dotted line.

μ_{H} as $\theta = \frac{k_{\mathrm{B}}T}{N_0}\frac{\partial}{\partial\mu_{\mathrm{H}}}\log\Xi$, where N_0 is the total number of adsorption sites. When there are many adsorption sites, it is impossible to calculate the grand partition function analytically, considering configurational possibilities. However, if there are a few dominant adsorption sites, we may obtain the approximate expression of the coverage by neglecting the configurational restrictions. In the case, the hydrogen coverage θ at the particular adsorption site is written as

$$\theta = \frac{1}{1+\exp\left(-\frac{\Delta E_{\mathrm{ad}}(T,P)/n_{\mathrm{H}}}{\mathrm{k_B}T}\right)}. \tag{9}$$

Here $\Delta E_{\mathrm{ad}}(T,P)$ is the adsorption energy of the H atoms at the particular site defined in Eq. (2). It is of note that the expression (9) is based on the assumption that the surface is in equilibrium with the gas phase, ignoring kinetic effects such as desorption barriers. More elaborate determination of the coverage remains for the future.

In the present work, we focus on the adsorption structure with the largest adsorption energy per H atom $\Delta E^0_{\mathrm{ad}}/n_{\mathrm{H}}$ for each step edge. We have also examined the coverage on the (0001) surface terrace. The adsorption energy on the terrace has been calculated using the H-terminated slab model with (1×1) lateral cell. Figure 8 shows the calculated hydrogen coverages of each step and the (0001) terrace in the temperature range of $T = 1200$ °C–1800 °C under H-rich conditions ($P_H = 0.25$ atm). This circumstance corresponds to typical HCVD growth conditions [8,9]. It is found that the coverage at the C1 step is the highest and that at the Si3 step is the lowest in this temperature range. At growth temperature of around 1625 °C [8,9], almost all of the C1 steps remain covered with H, and there are still H atoms at about half of the adsorption sites in the (0001) terrace. Most of the H atoms at the Si3 steps are desorbed and the pristine Si3 structure appears. For the Si2, C2, and SC steps, they show similar behavior of the coverages and their values are clearly lower than that on the (0001) terrace.

The difference in hydrogen coverage among those adsorption sites certainly provides basics to discuss the mechanism of the step-flow growth, since the H atoms which annihilate dangling bonds prevent the reaction sites from incorporating Si and C species and then reduce the growth rate. In the SC straight step under Si-poor conditions, the Si and C species are

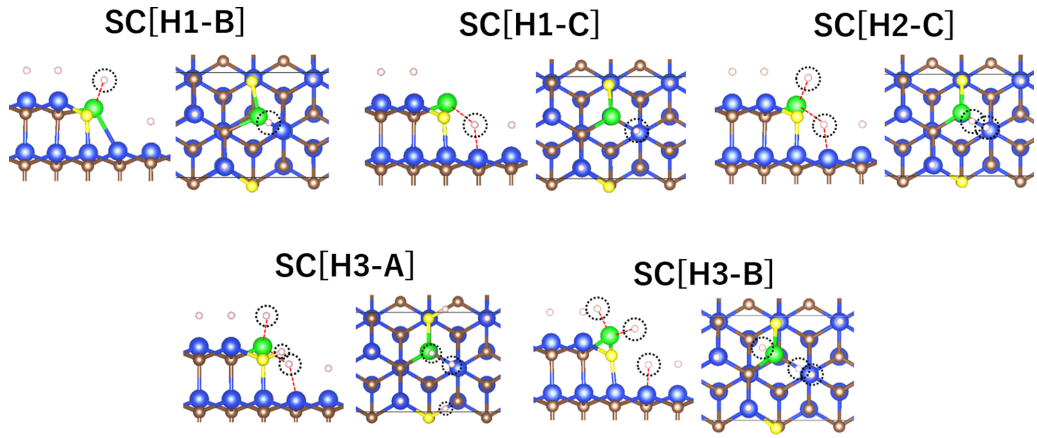

FIG. 11. Side (left) and top (right) views of the optimized local atomic structures of the geometry-optimized H-adsorbed SC steps with the adsorption energy about a half eV or less (Table I). The color code denoting atomic species is the same as in Fig. 10. H atoms adsorbed on the step edge are circled by the black dotted line.

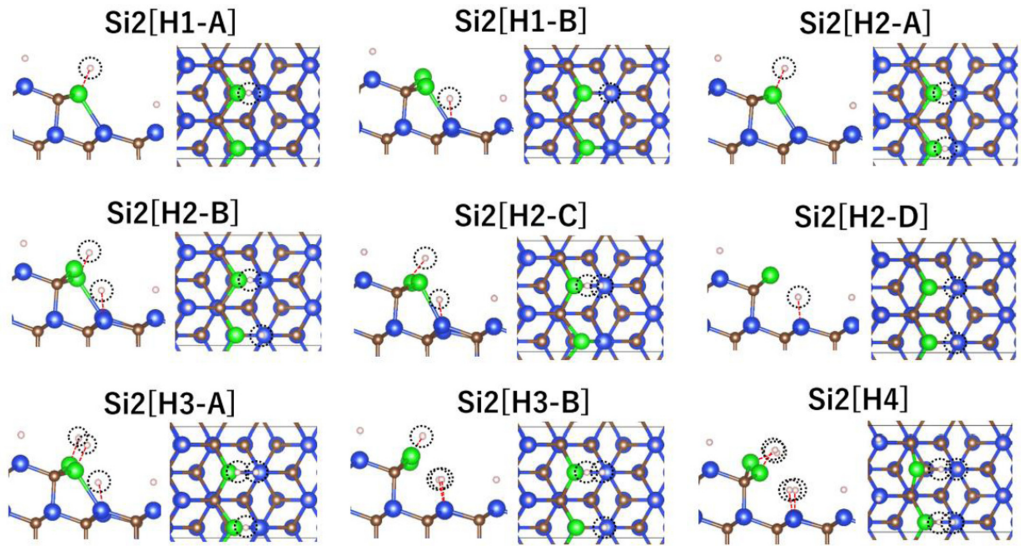

FIG. 12. Side (left) and top (right) views of the local atomic structures of the geometry-optimized H-adsorbed Si2 steps. The color code is the same as in Fig. 11. H atoms adsorbed on the step edge are circled by the black dotted line.

incorporated into the SC steps rather than the terraces because the hydrogen coverage of SC ($\theta_{\mathrm{SC}} = 0.10$ at $T = 1625$ °C) is lower than that on the terraces ($\theta_{\mathrm{terrace}} = 0.45$ at $T = 1625$ °C). In the Si2 + Si3 zigzag step edge under Si-rich condition, the Si and C species are expected to be incorporated into the Si2 + Si3 step edges rather than on the terrace, since the hydrogen coverages at Si2 and Si3 ($\theta_{\mathrm{Si2}} = 0.17$, $\theta_{\mathrm{Si3}} = 0.001$ at $T = 1625$ °C) are lower than that on the terrace. In particular, it is expected that the C species are easily adsorbed at the Si3 step due to its extremely low hydrogen coverage. However, after C species are incorporated at the edge Si of the Si3 step, the step edge is converted to the C1 step. Taking this into account, the growth of the Si3 and C1 side of the zigzag step edge is rate limiting because of the quite high hydrogen coverage of the C1 step ($\theta_{C1} = 0.97$ at $T = 1625$ °C). On the other hand, the C2 step appears after C species are incorporated at the edge Si of the Si2 step. Since the coverages at Si2 and C2 are comparable ($\theta_{C2} = 0.13$ at $T = 1625$ °C), the growth of the Si2 and C2 side of the zigzag step edge proceeds constantly.

Our calculations show that the step toward the $\langle 11\bar{2}0\rangle$ direction is zigzag shaped under Si-rich conditions. Interestingly, the growth direction of such Si2 + Si3 zigzag-shaped step edge still depends on the ratio of the growth rates at the Si2/C2 side and the Si3/C1 side. When the growth takes place dominantly at the Si2/C2 side, the epitaxial growth along the $\langle 11\bar{2}0\rangle$ vicinal surface is realized only by the step flow of the Si2/C2 side. From a microscopic perspective, the Si2/C2 side proceeds in a direction along the $\langle 10\bar{1}0\rangle$ direction. As a result, the zigzag-shaped edge appears to flow in the

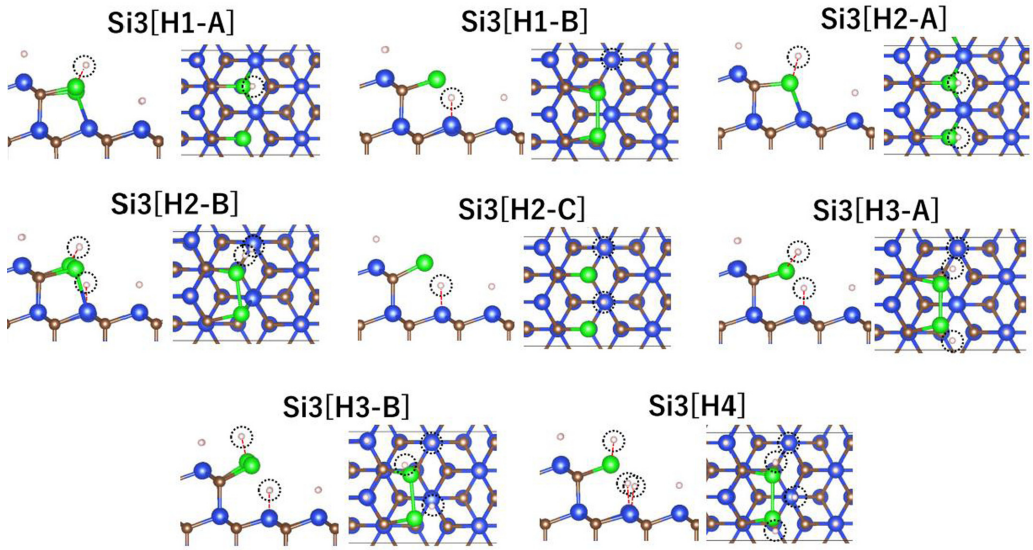

FIG. 13. Side (left) and top (right) views of the local atomic structures of the geometry-optimized H-adsorbed Si3 steps. The color code is the same as in Fig. 11. H atoms adsorbed on the step edge are circled by the black dotted line.

$\langle 11\bar{2}0\rangle$ direction with the positions of the growth-front kinks being changed alternately [Fig. 9(a)]. On the other hand, if the Si2/C2 side and Si3/C1 side have the same growth rate, the Si2 + Si3 zigzag-shaped step edge moves forward in the $\langle 11\bar{2}0\rangle$ direction with the positions of the growth-front kinks being unchanged. [Fig. 9(b)]. This is certainly observable in microscopic measurements, thus offering a tool to determine the chemical potentials.

IV. CONCLUSION

We have performed first-principles total-energy electronic-structure calculations, based on density-functional theory, that elucidate the atomic structures of H-adsorbed monobilayer-height atomic steps and their energetics of SiC(0001) surfaces. Among dozens of candidate structures of all the possible monobilayer steps with various H-adsorbed forms, we have identified the most favorable sites for H adsorption by optimizing the geometries and calculating the respective adsorption energies. The results obtained constitute a firm theoretical framework to discuss step morphology and then mechanisms of the epitaxial growth by chemical vapor deposition in which H atoms are ubiquitous. For instance, on the vicinal surface inclined toward the $\langle 11\bar{2}0\rangle$ direction, we have found that the straight step edges consisting of Si and C atoms are favorable in Si-rich conditions, while zigzag-shaped step edges consisting of Si edge atoms are favorable in Si-poor conditions, thus opening the possibility of controlling the step morphology by chemical potentials or growth conditions. Then we have calculated the hydrogen coverage at each step edge and on the terrace. The obtained variation in the H coverage for those step edges offers important information for the clear identification of reaction sites for the incorporation processes in the epitaxial growth. These findings unequivocally expand our understanding of the stages at which SiC epitaxial growth takes place and provide the basis to clarify the microscopic mechanism of the chemical reactions on stepped SiC(0001) surfaces during H-rich CVD.

ACKNOWLEDGMENTS

This work was supported by MEXT as "Program for promoting research on the supercomputer Fugaku" (quantum-theory-based multiscale simulations toward development of next-generation energy saving semiconductor devices: Project ID No. JPMXP1020200205) and as "Program for research and development of next-generation semiconductor to realize energy-saving society" (Project ID No. JPJ005357). The work was also supported by the grants-in-aid from MEXT under Contract No. 18H03873. Computations were performed at the Supercomputer Center, ISSP, The University of Tokyo, and the Research Center for Computational Science, the National Institute of Natural Sciences, and also with resources provided through the HPCI System Research project (Projects ID No. hp200122, ID No. hp210170, and ID No. hp220168).

APPENDIX: HYDROGEN-ADSORBED STEP-EDGE STRUCTURES OF SiC(0001) SURFACES

In this Appendix, we show several important but supplemental geometries of hydrogen-adsorbed step edges on SiC(0001) surfaces. They are (i) structures of a single-H adsorption at the SC step (Fig. 10), (ii) the adsorbed structures with many H atoms with smaller adsorption energies at the SC step (Fig. 11), (iii) all the stable H-adsorbed structures at the Si2 step (Fig. 12), and (iv) all the stable H-adsorbed structures at the Si2 step (Fig. 13).

[1] H. Baumhauer, Z. Kristallogr. **50**, 33 (1912).
[2] C. L. Burdick and E. A. Owen, J. Am. Chem. Soc. **40**, 1749 (1918).
[3] T. Kimoto and J. A. Cooper, *Fundamentals of Silicon Carbide Technology* (John Wiley & Sons, Singapore, 2014).
[4] For a review, see T. Kimoto and H. Watanabe, Appl. Phys. Exp. **13**, 120101 (2020).
[5] See, e.g., *Advances in the Understanding of Crystal Growth Mechanisms*, edited by T. Nishinaga, K. Nishioka, J. Harada, A. Sasaki, and H. Takei, (Elsevier, New York, 1997).
[6] H. Matsunami and T. Kimoto, Mater. Sci. Eng., R **20**, 125 (1997).
[7] F. la Via, G. Galvagno, G. Foti, M. Mauceri, S. Leone, G. Pistone, G. Abbondanza, A. Veneroni, M. Masi, and G. L. Valente, Chem. Vap. Deposiiton **12**, 509 (2006).
[8] Y. Daigo, S. Ishii, and T. Kobayashi, Jpn. J. Appl. Phys. **58**, SBBK06 (2019).
[9] K. Chokawa, Y. Daigo, I. Mizushima, T. Yoda, and K. Shiraishi, Jpn. J. Appl. Phys. **60**, 085503 (2021).
[10] T. Kimoto and H. Matsunami, J. Appl. Phys. **75**, 850 (1994).
[11] K. Seino and A. Oshiyama, Appl. Phys. Exp. **13**, 015506 (2020).
[12] K. Seino and A. Oshiyama, Phys. Rev. B **101**, 195307 (2020).
[13] P. Hohenberg and W. Kohn, Phys. Rev. **136**, B864 (1964).
[14] W. Kohn and L. J. Sham, Phys. Rev. **140**, A1133 (1965).
[15] K. Sawada, J.-I. Iwata, and A. Oshiyama, Appl. Phys. Lett. **104**, 051605 (2014).
[16] K. Sawada, J.-I. Iwata, and A. Oshiyama, Phys. Rev. B **93**, 235421 (2016).
[17] M. Saito and A. Oshiyama, Phys. Rev. Lett. **73**, 866 (1994).
[18] J.-I. Iwata, K. Shiraishi, and A. Oshiyama, Phys. Rev. B **77**, 115208 (2008).
[19] T. Ueda, H. Nishino, and H. Matsunami, J. Cryst. Growth **104**, 695 (1990).
[20] S. Tanaka, R. Kern, R. F. Davis, J. F. Wendelken, and J. Xu, Surf. Sci. **350**, 247 (1996).
[21] S.-I. Nakamura, T. Kimoto, H. Matsunami, S. Tanaka, N. Teraguchi, and A. Suzuki, Appl. Phys. Lett. **76**, 3412 (2000).
[22] S. Nie, C. D. Lee, R. M. Feenstra, Y. Ke, R. P. Devaty, W. J. Choyke, C. K. Inoki, T. S. Kuan, and G. Gu, Surf. Sci. **602**, 2936 (2008).
[23] G. Kresse and J. Hafner, Phys. Rev. B **47**, 558 (1993).
[24] G. Kresse and J. Hafner, Phys. Rev. B **49**, 14251 (1994).
[25] G. Kresse and J. Furthmüller, Phys. Rev. B **54**, 11169 (1996).
[26] G. Kresse and D. Joubert, Phys. Rev. B **59**, 1758 (1999).

[27] J. P. Perdew, K. Burke, and M. Ernzerhof, Phys. Rev. Lett. **77**, 3865 (1996).
[28] P. E. Blöchl, Phys. Rev. B **50**, 17953 (1994).
[29] H. J. Monkhorst and J. D. Pack, Phys. Rev. B **13**, 5188 (1976).
[30] C. H. Park, B.-H. Cheong, K.-H. Lee, and K. J. Chang, Phys. Rev. B **49**, 4485 (1994).
[31] K. Momma and F. Izumi, J. Appl. Crystallogr. **44**, 1272 (2011).
[32] Y. Kangawa, T. Ito, A. Taguchi, K. Shiraishi, and T. Ohachi, Surf. Sci. **493**, 178 (2001).
[33] Y. Kangawa, T. Ito, Y. S. Hiraoka, A. Taguchi, K. Shiraishi, and T. Ohachi, Surf. Sci. **507**, 285 (2002).
[34] Y. Kangawa, Y. Matsuo, T. Akiyama, T. Ito, K. Shiraishi, and K. Kakimoto, J. Cryst. Growth **300**, 62 (2007).
[35] For a review, see, Y. Kangawa, T. Akiyama, T. Ito, K. Shiraishi, and T. Nakayama, Materials **6**, 3309 (2013).
[36] D. J. Chadi, J. Vac. Sci. Technol., A **5**, 834 (1987).
[37] M. D. Pashley, Phys. Rev. B **40**, 10481 (1989).
[38] K. M. Bui, K. Shiraishi, and A. Oshiyama, Appl. Surf. Sci. **557**, 149542 (2021).